

**Cloud property retrievals for climate monitoring:  
implications of differences between SEVIRI on  
METEOSAT-8 and AVHRR on NOAA-17**

**R.A. Roebeling, A.J. Feijt and P. Stammes**

Royal Netherlands Meteorological Institute (KNMI), De Bilt, The Netherlands

R.A. Roebeling, A.J. Feijt and P. Stammes, Royal Netherlands Meteorological Institute (KNMI),  
P.O. Box 201, 3730 AE De Bilt, the Netherlands. (roebelin@knmi.nl; feijt@knmi.nl;  
stammes@knmi.nl)

**Abstract.** In the framework of the Satellite Application Facility on Climate Monitoring (CM-SAF) an algorithm was developed to retrieve Cloud Physical Properties (CPP) from the Spinning Enhanced Visible and Infrared Imager (SEVIRI) onboard the Meteosat Second Generation (METEOSAT-8) and the Advanced Very High Resolution Radiometer (AVHRR) onboard the National Oceanic and Atmospheric Administration (NOAA) satellites. This paper presents the CPP algorithm and determines if SEVIRI can be used together with AVHRR to build a consistent and accurate dataset of Cloud Optical Thickness (COT) and Cloud Liquid Water Path (CLWP) over Europe for climate research purposes. After quantifying the differences in 0.6 and 1.6  $\mu\text{m}$  operational calibrated reflectances of SEVIRI and AVHRR a recalibration procedure is proposed to normalize and absolutely calibrate these reflectances. The effects of recalibration, spatial resolution and viewing geometry differences on the SEVIRI and AVHRR cloud property retrievals are evaluated.

The intercomparison of 0.6 and 1.6  $\mu\text{m}$  operationally calibrated reflectances indicates  $\sim 6$  and  $\sim 26\%$  higher reflectances for SEVIRI than for AVHRR. These discrepancies result in retrieval differences between AVHRR and SEVIRI of  $\sim 8\%$  for COT and  $\sim 60\%$  for CLWP. Due to recalibration these differences reduce to  $\sim 5\%$ , while the magnitude of the median COT and CLWP values of AVHRR decrease  $\sim 2$  and  $\sim 60\%$  and the SEVIRI values increase  $\sim 10$  and  $\sim 55\%$ , respectively. The differences in spatial resolution and viewing geometry slightly influence the retrieval precision. Thus, the CPP algorithm can be used to build a consistent and high quality dataset of SEVIRI and AVHRR retrieved cloud properties for climate research purposes, provided the instrument reflectances are recalibrated, preferably guided by the satellite operators.

## 1. Introduction

Accurate information on cloud properties and their spatial and temporal variations are of great importance for climate studies. Clouds strongly modulate the energy balance of the Earth and its atmosphere through their interaction with solar and thermal radiation [Cess *et al.*, 1989]. Despite their importance, clouds are represented in a rudimentary way in climate and weather forecast models and contribute largely to the uncertainty in climate predictions. To improve the understanding of cloud processes and their representations in models, the Intergovernmental Panel on Climate Change (IPCC) calls for more measurements on cloud properties [IPCC TAR, 2001]. The radiative behavior of clouds depends predominantly on cloud physical properties such as thermodynamic phase, optical thickness and droplet effective radius. Satellites provide useful information on global cloud statistics and radiation budget. With the launch of Meteosat Second Generation (METEOSAT-8) in August 2002 a high quality data sets of cloud physical properties can be generated on a large scale (Earth disk covering Europe and Africa) at high temporal resolution of 15 minutes.

Several methods have been developed to retrieve cloud optical thickness and effective radius from satellite radiances at wavelengths in the non-absorbing visible and the moderately absorbing near infrared part of the spectrum [Nakajima and King, 1990; Han *et al.*, 1994; Nakajima and Nakajima, 1995; Watts *et al.*, 1998; Jolivet and Feijt, 2005; King *et al.*, 2004]. The principle of these methods is that the cloud reflectance at the visible wavelength is primarily a function of cloud optical thickness, while the reflectance at the near infrared wavelength is primarily a function of cloud particle size. The methods differ mainly in the choice of the satellite, the applied visible and near-infrared wavelengths and the interpolation and iteration scheme that is used for the retrieval of cloud physical properties. Nakajima and King [1990] use for their

retrievals a single non-absorbing visible wavelength (0.75  $\mu\text{m}$ ) and two absorbing near-infrared wavelengths (2.1 or 3.8  $\mu\text{m}$ ). The two absorbing near-infrared wavelengths are used to reduce the ambiguity in deriving the effective radius for optically thin clouds. For the Moderate Resolution Imaging Spectroradiometer (MODIS) Airborne Simulator (MAS) *King et al.* [2004] use the 0.87, 1.62 and 2.13  $\mu\text{m}$  channels for their retrieval of optical thickness and effective radius. Radiative Transfer Model (RTM) simulations of cloud reflectances, for predefined physical properties at given viewing geometries, are used to relate observed radiances to cloud physical properties. In principle the accuracy of the retrieved cloud properties depends, among others, on the surface albedo, 3D cloud effects, multi-layer cloud effects, the presence of aerosols and the representativeness of the assumed phase function. *Roebeling et al.*, [2005] assessed for commonly used RTMs the differences between RTM simulations of narrow-band visible and near-infrared radiances. They showed that not all RTMs are accurate enough for cloud property retrievals. Finally, there are a number of issues that depend on the satellite characteristics, i.e. instrument calibration, spectral response function, width of the spectral window, spatial resolution and viewing geometry.

So far little experience exists on the application of 1.6  $\mu\text{m}$  radiances for the retrieval of cloud physical properties, and the application of these methods on radiances of the Spinning Enhanced Visible and Infrared Imager (SEVIRI) on METEOSAT-8. The purpose of this study is to determine the accuracy and comparability of SEVIRI and AVHRR retrieved cloud physical properties from 0.6 and 1.6  $\mu\text{m}$  radiances, using the Cloud Physical Properties algorithm (CPP) of the Satellite Application Facility on Climate Monitoring (CM-SAF) of the European Organization for the Exploitation of Meteorological Satellites (EUMETSAT). The CM-SAF aims to generate and archive high quality data sets satellite products relevant for climate research for a region

covering Europe and Africa using EUMETSAT and National Oceanic and Atmospheric Administration (NOAA) satellites [Woick *et al.*, 2002]. The CM-SAF is complementary in goal to the International Satellite Cloud Climatology Project (ISCCP). The ISCCP aims to provide a global data set of monthly averaged cloud products to improve understanding and modeling of the role of clouds in climate [Rossow and Schiffer, 1991]. The ISCCP products have a lower temporal and spatial resolution than the regional cloud products of the CM-SAF, but offer the most complete and self-consistent set of calibrations and cloud properties from meteorological satellites over the period 1983 until 2002 [Rossow and Schiffer, 1999]. In this paper SEVIRI retrieved cloud physical properties are compared to validated cloud physical properties retrieved from the Advanced Very High Resolution Radiometer (AVHRR) of NOAA-17 [Jolivet and Feijt, 2005]. This comparison is done for cloud physical properties retrieved from reflectances that are calculated with the operational calibrations provided by the satellite operators and from recalibrated reflectances. Much attention is given to recalibration because that is prerequisite to build a consistent dataset of cloud properties retrieved from different satellites for climate monitoring. In order to explain the observed differences between SEVIRI and AVHRR retrieved cloud physical properties for an area over North Western Europe, an analysis is made of the effects of differences in calibration, spatial resolution and viewing geometry. The selected area covers a sub-section of the CM-SAF baseline area.

The outline of this paper is as follows. In section 2, the techniques that are used to calibrate reflectances and the CPP algorithm are described. This algorithm is used to retrieve cloud optical thickness (COT) and cloud liquid water path (CLWP). The study procedure and the results of the comparison of SEVIRI and AVHRR reflectances for the 0.6 and 1.6  $\mu\text{m}$  channels are presented in Section 3. In Section 4, the study procedure and the results of the intercomparison of SEVIRI and

AVHRR retrieved COT and CLWP is presented. The effects of the differences between SEVIRI and AVHRR in spatial resolution and viewing conditions on the retrieved COT and CLWP are illustrated in section 5. Finally, in section 6, the results are summarized and conclusions are drawn.

## 2. Methods

### *a. Satellite data*

The National Oceanic and Atmospheric Administration (NOAA) operates a series of polar orbiting satellites that carry the AVHRR instrument. The NOAA satellites circle the Earth 14 times per day at an altitude of about 833 km. The AVHRR instrument comprises six channels at wavelengths between 0.5 and 12.0  $\mu\text{m}$ . The NOAA-17 satellite, which is used for the present study, was launched in 2002.

Meteosat Second Generation is a new series of European geostationary satellites that is operated by EUMETSAT. In 2002 the first Meteosat Second Generation satellite (METEOSAT-8) was launched successfully. METEOSAT-8 is a spinning stabilized satellite that carries the 12-channel SEVIRI instrument with 11 channels at wavelengths between 0.6 and 14  $\mu\text{m}$  and one high resolution visible channel. SEVIRI and AVHRR have several comparable channels. Table 1 summarizes the spatial resolution and the spectral bands of the visible and near-infrared SEVIRI and AVHRR channels. Note that the 1.6  $\mu\text{m}$  channel of AVHRR on NOAA-17 is only active during daytime, while the 3.8  $\mu\text{m}$  channel is active during nighttime. All SEVIRI channels are operated simultaneously.

*b. Operational radiance calibration*

The SEVIRI and AVHRR instruments are not equipped with an onboard calibration device for the shortwave channels. Therefore the calibration of the shortwave channels of both radiometers is done pre-launch. Since the shortwave channels are known to degrade with time, it is necessary to monitor post-launch sensor degradation. Both EUMETSAT and NOAA use vicarious calibrations techniques for post-launch calibration. These techniques compare simulated Top Of Atmosphere (TOA) radiances with observed TOA Earth radiances for radiometrically stable terrestrial calibration target sites, such as bright desert targets [Govaerts and Clerici, 2004a; Rao and Chen, 1995]. According to Govaerts and Clerici [2004a] the accuracy of the vicarious calibration of the SEVIRI visible and near-infrared channels is expected to be about 5%, provided sufficient calibration targets and data are used. For AVHRR on NOAA-17 only pre-launch calibration coefficients are available. Currently NOAA does not provide official post-launch calibrations coefficients for the AVHRR solar channels on NOAA-17. Preliminary post-launch calibrations for NOAA-17/AVHRR indicate that the pre-launch calibration over-estimates the reflectances at 0.6  $\mu\text{m}$  and under-estimates those at 1.6  $\mu\text{m}$  by a few percent [Wu and Michael, 2003].

*c. Spectral response functions*

The SEVIRI and AVHRR instruments differ slightly in spectral response functions and bandwidth. Figure 1 shows that the spectral response functions of the 0.6  $\mu\text{m}$  channels of SEVIRI and AVHRR are very similar with a central wavelength of  $\sim 0.63 \mu\text{m}$  and bandwidth of  $\sim 0.58\text{-}0.70 \mu\text{m}$ . Larger differences are present between the 1.6  $\mu\text{m}$  channels of SEVIRI and AVHRR.

The central wavelengths of AVHRR 1.6  $\mu\text{m}$  channel ( $\sim 1.60 \mu\text{m}$ ) differs about  $0.05 \mu\text{m}$  with the central wavelength of the SEVIRI channel ( $\sim 1.65 \mu\text{m}$ ), whereas the bandwidth of the SEVIRI 1.6  $\mu\text{m}$  channel ( $\sim 1.56\text{--}1.72 \mu\text{m}$ ) is almost twice the width of the AVHRR channel ( $\sim 1.57\text{--}1.64 \mu\text{m}$ ). Since the TOA reflectance of Earth scenes varies with wavelength, the SEVIRI and AVHRR reflectances may differ due to differences in spectral response functions and bandwidth. Figure 2 presents examples of SCIAMACHY/ENVISAT measured TOA reflectance spectra for five typical scenes (ocean, vegetation, desert, liquid cloud and cirrus cloud) [Stammes *et al.*, 2005]. The gray blocks in Figure 2 indicate the positions of the 0.6 and 1.6  $\mu\text{m}$  channel of SEVIRI and AVHRR. The figure clearly demonstrates that the TOA reflectances of the five scenes are not spectrally gray for the SEVIRI and AVHRR channels. The five SCIAMACHY spectra were convoluted with the SEVIRI and AVHRR spectral response functions to translate these spectra for both instruments to channel reflectances at 0.6 and 1.6  $\mu\text{m}$ . Table 2 shows that the resulting SEVIRI and AVHRR channel reflectances at 0.6  $\mu\text{m}$  differ less than  $+2.1\%$  for the five SCIAMACHY spectra. The differences at 1.6  $\mu\text{m}$  are significantly larger, up to  $+11.2\%$  for the thick ice cloud scene. This large difference is explained by the strong decrease in absorption of ice crystals between 1.5 and 1.7  $\mu\text{m}$ .

#### *d. Recalibration*

The recalibration method of AVHRR and SEVIRI reflectances involves a normalization and absolute calibration procedure. The AVHRR reflectances are normalized to SEVIRI to reduce the calibration differences between both instruments. Subsequently, the normalized reflectances are calibrated to MODIS-Terra reflectances to obtain absolutely calibrated reflectances.

Although AVHRR and SEVIRI have the 0.6 and 1.6  $\mu\text{m}$  channel in common, there are small differences in spectral response function and bandwidth. *Rossow and Schiffer* [1999] have shown that normalization of calibrations of different radiometers is prerequisite to construct a uniform regional or global dataset of cloud physical properties from different satellites over a long time period. In this paper the normalization technique of *Heidinger et al.* [2002] is used, which employs co-located MODIS reflectances to calibrate AVHRR reflectances, by matching the frequency distributions of reflectance from AVHRR to MODIS.

To construct an accurate dataset of cloud physical properties absolute calibration is essential. The vicarious calibrations techniques used by EUMETSAT and NOAA provide post-launch absolute calibrations, with an accuracy of about 5% [*Govaerts and Clerici*, 2004a]. A better way to absolutely calibrate the normalized AVHRR and SEVIRI reflectances is to cross-calibrate with MODIS–Terra observed reflectances. The MODIS–Terra instrument has in-flight absolute calibration methods for the shortwave channels that have an expected uncertainty of about 2% for the reflectances [*Guenther et al.*, 1998].

*e. Retrieval of cloud physical properties*

The principle of methods to retrieve cloud physical properties is that the reflectance of clouds at a non-absorbing wavelength in the visible region (0.6 or 0.8  $\mu\text{m}$ ) is strongly related to the optical thickness and has very little dependence on particle size, whereas the reflectance of clouds at an absorbing wavelength in the near-infrared region (1.6 or 3.8  $\mu\text{m}$ ) is primarily related to particle size. Note that the retrieval of particle size from near-infrared reflectances is weighted towards the upper part of the cloud [*Platnick*, 2001]. The average penetration depth of reflected

photons is affected by the amount of absorption, which depends on wavelength, particle type and size. The reflectance at 1.6  $\mu\text{m}$  is found to be mainly a function of particle size for clouds with an optical thickness higher than about 8, whereas the reflectance at 3.8  $\mu\text{m}$  is more suited for the retrieval of cloud particle size for thin clouds ( $\text{COT} > \sim 2$ ) [Rosenfeld, 2004; Watts *et al.*, 1998]. However, the 3.8  $\mu\text{m}$  channel has a number of disadvantages that may lead to significant errors: (1) the radiance observed at 3.8  $\mu\text{m}$  consists of both reflected solar radiance and thermal emitted radiance, (2) the signal to noise ratio is lower due to the approximately 4 times lower solar irradiance at 3.8  $\mu\text{m}$  than at 1.6  $\mu\text{m}$ , and finally (3) because the 3.8  $\mu\text{m}$  retrievals represent the particle size of the upper part of the cloud these retrievals will be less representative for radiative transfer in optically thick clouds [Feijt *et al.*, 2004].

The Doubling Adding KNMI (DAK) radiative transfer model is used to generate the Look Up Tables (LUTs) of simulated cloud reflectances. DAK is developed for line-by-line or monochromatic multiple scattering calculations at UV, visible and near infrared wavelengths in a horizontally homogeneous cloudy atmosphere using the doubling-adding method [De Haan *et al.*, 1987; Stammes, 2001]. The clouds are assumed to be plane-parallel and embedded in a multi-layered Rayleigh scattering atmosphere.

The algorithm we utilize to retrieve cloud physical properties is based on reflectances at visible (0.6  $\mu\text{m}$ ) and near-infrared (1.6  $\mu\text{m}$ ) wavelengths. Figure 3 presents a flowchart of the CPP algorithm for the retrieval of COT, particle size and CLWP. In this version (1.0) of the algorithm the pixel is assumed cloudy if the observed reflectance at 0.6  $\mu\text{m}$  is higher than the simulated clear sky reflectance over the observed surface. Moreover this version uses assumed surface albedos, which are 0.10 over land and 0.05 over ocean at 0.6  $\mu\text{m}$  and 0.15 over land and 0.05 over ocean at 1.6  $\mu\text{m}$ . The COT and particle size are retrieved for cloudy pixels in an

iterative manner, by simultaneously comparing satellite observed reflectances at visible (0.6  $\mu\text{m}$ ) and near-infrared (1.6  $\mu\text{m}$ ) wavelengths to LUTs of RTM simulated reflectances for given optical thicknesses and particle sizes [Watts *et al.*, 1998; Jolivet and Feijt, 2005]. Table 3 summarizes the governing characteristics of the cloudy atmosphere, together with information about intervals of cloud properties and viewing geometries used for the DAK simulations. During the iteration the COT values that are retrieved at the 0.6  $\mu\text{m}$  channel are used to update the retrieval of particle size at the 1.6  $\mu\text{m}$  channel. This iteration process continues until the retrieved cloud physical properties converge to stable values. The interpolation between cloud physical properties in the LUTs is done with polynomial interpolation for COT values and linear interpolation for particle size. For optically thin clouds (COT < 8) the retrieved particle size values are unreliable. For these clouds an assumed climatological averaged effective radius is used that is 8  $\mu\text{m}$  for water clouds and 35  $\mu\text{m}$  for ice clouds, which is close to the values used by Rossow and Schiffer [1999]. To obtain a smooth transition between assumed and retrieved effective radii a weighting function is applied on the effective radius retrievals of clouds with COT values between zero and eight. The retrieval of cloud thermodynamic phase is done simultaneously with the retrieval of COT and particle size. The phase “ice” is assigned to pixels with a Cloud Top Temperature (CTT) lower than 265 K for which the 0.6  $\mu\text{m}$  and 1.6  $\mu\text{m}$  reflectances correspond to DAK simulated reflectances for ice clouds. The remaining cloudy pixels are considered water clouds.

The droplet effective radius ( $r_e$ ) is the adequate parameter to represent the radiative properties of a size distribution of water particles that is given by [Hansen and Hovenier, 1974]:

$$r_e = \frac{\int_0^{\infty} r^3 n(r) dr}{\int_0^{\infty} r^2 n(r) dr} \quad (1)$$

where  $n(r)$  is the particle size distribution and  $r$  is the particle radius. This definition is used to retrieve the effective radius for water clouds between 1 and 24  $\mu\text{m}$ . For ice clouds we assume a homogeneous distribution of C1 and C2 type imperfect hexagonal ice crystals from the COP data library of optical properties of hexagonal ice crystals [Hess *et al.*, 1998]. Knap *et al.* [2005] demonstrated that these crystals could be used to give adequate simulations of total and polarized reflectances of ice clouds.

The CTT is calculated from 10.8  $\mu\text{m}$  brightness temperatures and the emissivity of the cloud ( $\varepsilon_\lambda$ ). The  $\varepsilon_\lambda$  is calculated from the cloud optical thickness at wavelength  $\lambda$  ( $\tau_\lambda$ ) with the following equation [Minnis *et al.*, 1993]:

$$\varepsilon_\lambda = 1 - \exp\left(\frac{-\tau_\lambda}{\cos\theta}\right) \quad (2)$$

where  $\cos\theta$  is the cosine of the viewing zenith angle. The (absorbing) cloud optical thickness in the infrared ( $\tau_{ir}$ ) is related to the (scattering) cloud optical thickness in the visible ( $\tau_{vis}$ ). This relationship depends on particle size and particle thermodynamic phase. For large water and ice particles  $\tau_{ir}$  is about  $0.5 \tau_{vis}$ .

The CLWP is computed from the retrieved cloud optical thickness at wavelength at 0.6  $\mu\text{m}$  (denoted as  $\tau_{vis}$ ) and droplet effective radius ( $r_e$ ) as follows [Stephens, 1978]:

$$CLWP = \frac{2}{3} \tau_{vis} r_e \rho_l \quad (3)$$

where  $\rho_l$  is the density of liquid water. For ice clouds the CLWP is retrieved with an assumed effective radius of 30  $\mu\text{m}$  for C1 ice crystals and 40  $\mu\text{m}$  for C2 ice crystals.

### 3. Comparison between SEVIRI and AVHRR reflectances

#### a. Study procedure

SEVIRI and AVHRR reflectances at 0.6 and 1.6  $\mu\text{m}$  were compared to investigate the calibration of SEVIRI. To minimize differences in viewing geometry, an area over Central Africa close to the equator (5°W to 5°E and 5°N to 18°N) was chosen for comparing the SEVIRI and AVHRR images. For AVHRR we used the pre-launch calibration coefficients provided by NOAA, whereas for SEVIRI we used the post-launch calibration coefficients that EUMETSAT provided at the end of the commissioning phase. The reflectances ( $\rho_\lambda$ ) were calculated by:

$$\rho_\lambda = \frac{\pi L_\lambda}{F_\lambda \cos \theta_0} \quad (4)$$

where  $L_\lambda$  is the Earth radiance reflected in the direction of the satellite,  $F_\lambda$  is the incoming solar irradiance received at the top of the atmosphere perpendicular to the solar beam, and  $\theta_0$  is the solar zenith angle.

During the period September 2004 – December 2004 nine SEVIRI and AVHRR images with about equal acquisition times were selected. The images were re-projected to a Mercator projection and re-sampled to a similar spatial resolution. The comparison of re-projected AVHRR

and SEVIRI images revealed small differences due to different observation times and collocation errors. To reduce the collocation errors the AVHRR images were shifted within a 5x5 pixel box to find the maximum correlation with the SEVIRI images. Finally, SEVIRI and AVHRR pixels were selected with zenith viewing angles smaller than  $30^\circ$  and scattering angles between  $140^\circ - 175^\circ$  and  $120^\circ - 130^\circ$ . Pixels with scattering angles close to  $180^\circ$  and  $137^\circ$  were excluded to eliminate pixels that are affected by the glory and the rainbow, respectively. Contour plots and cumulative frequency distributions were analyzed to assess the differences between SEVIRI and AVHRR reflectances at 0.6 and 1.6  $\mu\text{m}$ .

#### *b. Results*

Figure 4 shows an example of a SEVIRI and AVHRR 1.6  $\mu\text{m}$  image for the area over Central Africa that is used for the reflectance comparison. The selected images comprise typical scenes that can be observed over Africa, i.e. semi-arid, desert-like, sea surfaces, water and ice clouds. The impact of the difference in spatial resolution and channel characteristics between AVHRR ( $1 \times 1 \text{ km}^2$  at nadir) and SEVIRI ( $3 \times 3 \text{ km}^2$  at nadir) can be seen clearly from the images. Typical features, such as Lake Volta in Ghana, can be recognized on both images, but the broken clouds field over Southwest Ghana that can be distinguished on the AVHRR image (see circle) appears on the SEVIRI image as homogeneous cloud field. The arrows on the images indicate an area with ice clouds over a desert-like area in Mali, which appear as dark spots due to the strong absorption of ice particles at 1.6  $\mu\text{m}$ .

Figures 5 and 6 present contour plots and cumulative frequency distributions of SEVIRI and AVHRR reflectances for the 0.6 and 1.6  $\mu\text{m}$  channel, respectively. For both channels the correlation between SEVIRI and AVHRR reflectances is high, the offsets of the regression

equations are close to zero and the correlation coefficients ( $r$ ) are 0.93 at 0.6  $\mu\text{m}$  and 0.95 at 1.6  $\mu\text{m}$ . At 0.6  $\mu\text{m}$  the SEVIRI reflectances are about 6% higher than the AVHRR reflectances. Considering the differences in spatial resolution, viewing conditions and time of overpass between SEVIRI and AVHRR, the differences at 0.6  $\mu\text{m}$  are within the uncertainty boundaries (see section 2). Larger differences are observed for the 1.6  $\mu\text{m}$  channel, where the slope of 0.79 indicates approximately 26% higher reflectances from SEVIRI than from AVHRR. It is very unlikely that these differences are due to the slight differences in viewing geometry between the two instruments. Such a difference would show up in the 0.6micron channel radiances too, which is not the case here. The analysis of SCIAMACHY scenes, presented in section 2, shows that the differences in bandwidth and spectral response function of the 1.6  $\mu\text{m}$  channel of SEVIRI and AVHRR could explain for reflectance difference between +0.7% for the desert scene and +11.2% for the thick ice cloud scene. Since the amount of ice clouds in the analyzed images is very low, the actual differences between the SEVIRI and AVHRR reflectances at 1.6  $\mu\text{m}$  are expected to be smaller than about 3%. However, it is more likely that the observed differences result from uncertainties in the SEVIRI and/or AVHRR calibration of the 1.6  $\mu\text{m}$  channel. The post-launch vicarious calibrations that were used for METEOSAT-8/SEVIRI have an expected accuracy of 5%. Moreover, *Govaerts and Clerici* [2004b] demonstrated that the calibration of the SEVIRI channels is stable and shows minor drift compared to the pre-launch calibration. Therefore it can be concluded that most of the uncertainties are probably in the NOAA-17/AVHRR pre-launch calibrations, which can be higher than 10%.

#### **4. Comparison between SEVIRI and AVHRR cloud physical properties**

*a. Study procedure*

The comparison of SEVIRI and AVHRR cloud properties retrievals was done with operationally calibrated reflectances and recalibrated reflectances. The operationally calibrated reflectances were used to investigate if these calibrations can be used to retrieve for water clouds COT and CLWP values with a similar accuracy from SEVIRI and AVHRR. The recalibrated reflectances were used to assess the effect of normalization and absolute calibration on the comparability and magnitude of SEVIRI and AVHRR retrievals of COT and CLWP.

The results from the reflectance intercomparison over Central Africa were used to normalize the AVHRR reflectances to SEVIRI. This normalization was done by matching AVHRR frequency distributions of reflectances to SEVIRI, which is in close analogy to the normalization method proposed by *Heidinger et al.* [2002]. The calibrations of AVHRR were matched to SEVIRI by increasing the reflectances of the 0.6  $\mu\text{m}$  channel with  $\sim 3\%$  and of the 1.6  $\mu\text{m}$  channel with  $\sim 22\%$ . These percentages differ from the results of the reflectance intercomparison over Central Africa with 3% at 0.6  $\mu\text{m}$  and 4% at 1.6  $\mu\text{m}$ , because the differences in spectral response function and width of the spectral window between both imagers are accounted for in the cloud property retrieval algorithm. In order to calibrate the normalized reflectances absolutely we used the results presented by *Doelling et al.* [2004]. They showed that the SEVIRI reflectances are about 8% lower at 0.6  $\mu\text{m}$  and 3% lower at 1.6  $\mu\text{m}$  than the MODIS–Terra reflectances, which are absolutely calibrated. In total the recalibration (normalization and absolute calibration) of AVHRR involved an increase of the reflectances at 0.6  $\mu\text{m}$  with 11% and at 1.6  $\mu\text{m}$  of 25%. Note that the recalibration method corrects for spectral response function, bandwidth and calibration differences between AVHRR and SEVIRI for spectrally gray scenes. No additional correction is applied for non-spectrally gray scenes such as ice clouds, for which the analysis of SCIAMACHY

reflectance spectra showed differences of about 11% due to the spectral response function and bandwidth of the 1.6 micron channels.

The comparison of COT and CLWP retrievals was done for an area of about 800 km x 900 km over the UK, the Netherlands and Germany ( 2.5°W to 11.0°E and 47.5°N to 57.0°N) for 35 images during the period 15 April - 14 May 2004. During the observation period the percentage of cloud free observations was about 10%. About 60% of the observed clouds were identified as water clouds and 20% as ice clouds. The processing was done with the CPP algorithm using operationally calibrated and recalibrated reflectances. The SEVIRI observations closest to the AVHRR overpass time were used. Because only half hourly SEVIRI images were available the SEVIRI and AVHRR overpass times differed less than 15 minutes. The SEVIRI and AVHRR retrieved cloud properties were re-projected to a Mercator projection of similar grid size. To reduce the collocation errors the AVHRR images were shifted within a 5x5 pixel box to find the maximum correlation with the SEVIRI images. Logarithmic averaging was used to calculate the mean COT during the observation period and account for the quasi-logarithmic relationship between cloud albedo and COT, using the following equation:

$$\overline{\tau_{vis}} = \exp\left(\frac{\sum_1^n \log(\tau_{vis}(i))}{n}\right) \quad (5)$$

where  $\overline{\tau_{vis}}$  is the logarithmically averaged COT,  $\tau_{vis}(i)$  is the COT value of an individual observation and  $n$  is the number of observations.

Frequency distributions of COT and CLWP retrievals were compared for individual observations and for the entire observation period to analyze the influence of the applied calibration on the median (50<sup>th</sup> percentile), the 95<sup>th</sup> percentile and the correlation coefficient of

SEVIRI and AVHRR retrievals. The main advantage of comparing frequency distributions is that the results are less affected by the collocation errors. The observed differences are caused by differences in instrument calibration, channel characteristics and spatial resolution. Moreover, there are differences that result from variations in the precision of cloud properties retrievals due to different viewing conditions.

*b. Results*

Figure 7 shows composite images of SEVIRI and AVHRR logarithmic averaged COT and averaged CLWP for both water and ice clouds for 35 images during the period 15 April - 14 May 2004. The composites are derived with the operational calibrations and represent the study area over North Western Europe that is used for this comparison study. Visual inspection reveals a high similarity of patterns and magnitude between SEVIRI and AVHRR retrieved COT values. However, SEVIRI retrieves about 50% lower CLWP values than AVHRR. For example, over the Southern UK the CLWP values vary between 150 and 300  $\text{g m}^{-2}$  for AVHRR and between 80 and 200  $\text{g m}^{-2}$  for SEVIRI.

Figure 8 presents for water clouds the frequency distributions of SEVIRI and AVHRR retrieved COT and CLWP over the observation period using the operational calibrations. Although the frequency distributions of COT are similar, the frequency of clouds with COT < 15 is about 15% higher for SEVIRI than for AVHRR, while the frequency of clouds with COT values between 25 and 40 is about 10% higher for AVHRR than for SEVIRI. The differences between the SEVIRI and AVHRR frequency distributions of CLWP are much larger. The frequency of clouds with CLWP < 50  $\text{g m}^{-2}$  is about 30% higher for SEVIRI than for AVHRR,

whereas for AVHRR the frequency of clouds with CLWP between 50 and 500 g m<sup>-2</sup> is about 20% higher than for SEVIRI. The major part of the differences between SEVIRI and AVHRR retrievals of CLWP arise from the about 20% higher reflectance of SEVIRI at 1.6 μm. The higher SEVIRI reflectances at the 1.6 μm will lead to the retrieval of smaller effective radii. Because the CLWP is approximated from the retrieved COT and droplet effective radius (equation 3) the differences in retrieved effective radius will directly affect the retrieval of CLWP. With the current large calibration differences between SEVIRI and AVHRR it is therefore not possible to derive comparable cloud properties from both instruments. Figure 9 shows that the SEVIRI and AVHRR frequency distributions match much better when the recalibrated reflectances are used. Both for COT and CLWP the frequencies differ less than 5%. Considering collocation errors and differences in spatial resolution and viewing conditions, the agreement between the recalibrated SEVIRI and AVHRR retrievals can be regarded satisfactory.

To analyze the differences between the individual SEVIRI and AVHRR retrievals over the observation period frequency distributions were compared. Figure 10 shows for SEVIRI and AVHRR the median COT and CLWP values for the 35 overpasses, using the operational calibrations. During the observation period the median COT values have a large day-to-day variability, which varies between 2 and 20. However, the SEVIRI and AVHRR median COT values are well correlated ( $r = 0.96$ ) and have a low standard deviation of differences (Std\_Diff = 1.5). Over the entire observation period the AVHRR median CLWP values are significantly larger than the SEVIRI values, with differences up to 120 g m<sup>-2</sup>. Although the SEVIRI and AVHRR median CLWP values correlate fairly well ( $r = 0.92$ ), the standard deviation of the differences of 33.6 g m<sup>-2</sup> is relatively high. Figure 11 shows that the median COT and CLWP values agree much better over the observation period after the recalibration than before (see

Figure 10). The biases between the SEVIRI and AVHRR retrievals of COT and CLWP do almost disappear. Moreover, the differences between SEVIRI and AVHRR retrievals are acceptably small, and vary between -3 and 3 for COT and between -30 and 30  $\text{g m}^{-2}$  for CLWP. The recalibration of the 1.6  $\mu\text{m}$  channel is the primary cause of the improved agreement between the CLWP values of both imagers because of the large correction (+25%) and the high sensitivity to particle size of the 1.6  $\mu\text{m}$  reflectances.

Table 4 and 5 summarize for SEVIRI and AVHRR the median, the 95<sup>th</sup> percentile, the correlation coefficient and the standard deviation of differences of COT and CLWP retrievals for water clouds over the observation period, using operationally calibrated and recalibrated reflectances. The recalibration of AVHRR and SEVIRI reflectances affects the results in two ways. First, the differences between the SEVIRI and AVHRR retrieved COT and CLWP values are strongly reduced due to normalizing the AVHRR reflectances to SEVIRI. Second, the magnitudes of the COT and CLWP values change due to adjusting the SEVIRI and AVHRR reflectances to MODIS-Terra. The biases between the SEVIRI and AVHRR median and 95<sup>th</sup> percentile COT and CLWP values are significantly smaller (< 5%) and the correlation coefficients are slightly higher (> 0.9) when recalibrated instead of operationally calibrated reflectances are used. Furthermore, the median and 95<sup>th</sup> percentile COT values increase for SEVIRI with about 10 and 65%, while for AVHRR the median decrease with about 2% and the 95<sup>th</sup> percentile increases with about 40%. The effect of recalibration on the magnitude of the CLWP values is larger. The SEVIRI median and 95<sup>th</sup> percentile CLWP values increase with about 55%, while for AVHRR the median value decreases with 60% and the 95<sup>th</sup> percentile value decreases with 10%.

A remarkable result is that despite the 11% increase of AVHRR reflectances at 0.6  $\mu\text{m}$  the median COT values decrease with about 2% after recalibration. Although the retrieval of COT is mainly dependent on the 0.6  $\mu\text{m}$  reflectances, the 1.6  $\mu\text{m}$  reflectances also affect the retrieved COT values. The dependence of COT on effective radius becomes noticeable, because the recalibration involved a significant 25% increase of 1.6  $\mu\text{m}$  reflectances. This dependence is largest for optically thin clouds (COT < 8). Figure 12 shows for two viewing geometries the relationship between simulated 0.6 and 1.6  $\mu\text{m}$  reflectances for various cloud optical thicknesses and particle sizes. In the figure the simulation results of both water clouds (effective radius 2–24  $\mu\text{m}$ ) and ice clouds (imperfect hexagonal crystals C1 and C2) are presented. The vertical arrows in the figure illustrate how a 25% increase in 1.6  $\mu\text{m}$  reflectances results in a decrease of cloud optical thickness values, whereas the horizontal arrows indicate that a 11% increase in 0.6  $\mu\text{m}$  reflectance results in an increase of COT values. It can be seen that recalibration of 0.6 and 1.6  $\mu\text{m}$  reflectances hardly changes the COT values for optically thin clouds, while the COT values for optically thick clouds increase. DAK simulations for other viewing geometries showed that the particle size dependence of the COT retrievals is larger for viewing geometries that correspond to scattering angles of the rainbow ( $\sim 137^\circ$ ) and the glory ( $\sim 180^\circ$ ).

## 5. Effects of other SEVIRI and AVHRR differences on cloud property retrievals

This section analyses the influence of the main sources of differences between SEVIRI and AVHRR on the retrieval of COT and CLWP over North Western Europe, which are: the instruments spatial resolution and viewing geometry.

### *a. Influence of spatial resolution*

Earlier studies have shown that differences in spatial resolution can cause systematic biases in retrieved cloud properties [Cahalan *et al.*, 1994; Wielicki and Parker, 1992; Davis *et al.*, 1997; Varnai and Marshak, 2001]. The nonlinear relationship between COT and reflectance can give an underestimation of COT values over dark surfaces as the spatial resolution decreases. Figure 9 shows that the SEVIRI and AVHRR frequency distributions of COT and CLWP have similar shape and minimum and maximum values. However, the lower tail of the distributions reveals differences that are probably related to spatial resolution. The left graph in Figure 13 shows that the frequency of thin clouds, with COT values between 1 and 4, is higher for SEVIRI than for AVHRR. It is suggested that these differences partly result from broken cloud fields that appear as homogeneous fields of thin clouds at the  $4 \times 7 \text{ km}^2$  resolution of SEVIRI, while at the  $1 \times 1 \text{ km}^2$  resolution of AVHRR these fields will show up either as cloud free or as clouds with COT values  $> 4$ . Figure 4 shows an example of such a cloud field over Southwest Ghana, which is marked by a circle. The right graph in Figure 13 shows that the differences between the SEVIRI and AVHRR distributions of COT reduce when the AVHRR data are resampled to the spatial resolution of SEVIRI over North Western Europe ( $4 \times 7 \text{ km}^2$ ). However, even after resampling part of the differences remain. It is suggested that these differences are caused by differences in viewing geometry. Since SEVIRI observes North Western Europe with larger viewing zenith angle ( $\sim 60^\circ$ ) than AVHRR, broken cloud fields tend to appear as homogeneous fields of optically thin clouds because SEVIRI observes cloud sides rather than cloudy and cloud free pixels. A similar comparison for CLWP revealed much smaller differences between the SEVIRI and AVHRR frequency distributions. A possible explanation for these smaller differences may be that SEVIRI retrieves for broken cloud fields lower COT values and simultaneously higher effective radii than AVHRR, which will have a compensating effect on the CLWP retrievals.

*b. Influence of viewing geometry*

*Loeb and Coakley* [1998] have shown that frequency distributions of COT values Marine status water clouds show very little change at relative azimuth angles in backward scattering direction ( $\phi = 120^\circ - 140^\circ$ ) and satellite and solar zenith angles  $< 60^\circ$ . However, in forward scattering directions ( $\phi = 10^\circ - 30^\circ$ ) the differences between frequency distributions of COT values are much larger and show a systematic drift in the peak COT as the viewing zenith angle increases.

Over North Western Europe SEVIRI and AVHRR retrievals of cloud physical properties take place for completely different viewing geometries. During the period 15 April until 14 May 2004 the peak scattering angle for AVHRR and SEVIRI was about  $140^\circ$ . The AVHRR viewing angles ranged between  $0^\circ$  and  $20^\circ$ , whereas the SEVIRI viewing zenith angles are larger than  $50^\circ$ . Furthermore, around noon SEVIRI is in the same plane as the sun, which makes the retrievals very sensitive to radiative transfer simulation flaws because the azimuthal difference is about  $180^\circ$ .

To investigate the dependence of our data set to viewing geometry Figure 14 presents the relationship between DAK simulated reflectances and viewing angles for various COT and effective radii values for water clouds. The range of viewing conditions used in the figure represent the mean conditions during the observation period over the Netherlands, which are an observation time of 10:30 UTC, an observation date of 1 May 2004, a solar zenith angle of about  $40^\circ \pm 3^\circ$  and relative azimuth angles between  $130^\circ$  and  $150^\circ$ . In our analysis the relative azimuth angle is used instead of the scattering angle, because the azimuth angle is independent from the

solar and viewing zenith angles. The sensitivity to small perturbations in viewing geometry is illustrated by the error bars, which give the standard deviation of mean reflectance due to variations of solar zenith angles ( $\pm 3^\circ$ ) and relative azimuth angles ( $\pm 10^\circ$ ). For the mean overpass time the main difference between SEVIRI and AVHRR geometries is the difference in satellite viewing zenith angle, which is about  $60^\circ$  for SEVIRI and generally between  $0^\circ$  and  $20^\circ$  for AVHRR. The figures clearly demonstrate that going from COT 1 to 128 the  $0.6 \mu\text{m}$  reflectance of a water cloud with an effective radius  $12 \mu\text{m}$  increases from about 0.08 to 0.92 for AVHRR and from 0.14 to 0.82 for SEVIRI. Compared to AVHRR this corresponds to a  $\sim 20\%$  reduction in the dynamic range of cloud reflectances for SEVIRI. A similar reduction in dynamic range is observed for the  $1.6 \mu\text{m}$  reflectances, where going from effective radius 24 to  $3 \mu\text{m}$  the reflectance of a cloud with optical thickness 128 increases from 0.42 to 0.82 for AVHRR and from 0.47 to 0.77 for SEVIRI. The error bars in the figures show that the uncertainty of the cloud property retrievals increases with viewing angle, but error bars larger than  $\sim 10\%$  do occur for viewing angles  $> 70^\circ$ . Simulations using larger solar zenith angles ( $> 50^\circ$ ) have shown that large error bars ( $> 10\%$ ) do occur at viewing zenith angles  $> 30^\circ$ . Because SEVIRI has a fixed viewing geometry these less favorable conditions will permanently affect the precision of SEVIRI based cloud property retrievals at higher latitudes. The large error bars at solar zenith angles  $> 50^\circ$  indicate that a lower precision of SEVIRI cloud property retrievals is expected at higher latitudes during early morning or late noon observations in summer, and throughout the day during the winter half-year. The viewing geometry analysis above is restricted to plane-parallel clouds and only gives qualitative information. Quantitatively the actual impact on retrievals may be different due to 3D cloud effects such as shadowing and horizontal photon transport.

## 6. Summary and Conclusions

This paper presented a comparison of SEVIRI and AVHRR retrievals of COT and CLWP from the CPP scheme that was developed in the framework of the CM-SAF. It was examined if SEVIRI and AVHRR can be used over North Western Europe to retrieve cloud properties with a similar accuracy. The selected area covered part of the CM-SAF baseline area where SEVIRI is used to generate a dataset of cloud properties for climate research purposes. It was shown that SEVIRI and AVHRR cloud properties differ significantly when the operational calibrations provided by the satellite operators are used. In order to quantify the differences in instrument calibration a direct comparison of the visible ( $0.6 \mu\text{m}$ ) and near-infrared ( $1.6 \mu\text{m}$ ) reflectances was done over Central Africa. The comparability of SEVIRI and AVHRR cloud properties over North Western Europe improved significantly when recalibrated reflectances are used. Finally, it was shown that other differences, such as viewing geometry and spectral and spatial resolution have little effect on the comparability of SEVIRI and AVHRR cloud properties.

The variations in SEVIRI and AVHRR reflectances showed a high level of agreement over Central Africa, with correlations coefficients of  $\sim 0.93$  at  $0.6 \mu\text{m}$  and  $\sim 0.95$  at  $1.6 \mu\text{m}$ . At  $0.6 \mu\text{m}$  SEVIRI observed  $\sim 5\%$  greater reflectances than AVHRR. The differences were much larger at  $1.6 \mu\text{m}$ , where SEVIRI observed  $\sim 20\%$  higher reflectances than the AVHRR. The analysis of SCIAMACHY observed TOA spectra showed that the  $0.6 \mu\text{m}$  channel reflectances of AVHRR and SEVIRI should differ less than  $2.5\%$ , whereas the  $1.6 \mu\text{m}$  channel reflectances should differ between  $\sim 2\%$  for a liquid water cloud and  $\sim 11\%$  for a cirrus cloud on the basis of their different spectral response functions. Since the calibration accuracy of the SEVIRI visible and near-

infrared channels is expected to be about 5%, and the first calibration reports show that the SEVIRI calibration is stable [Govaerts and Clerici, 2004b], most of the uncertainties are probably in the NOAA-17/AVHRR pre-launch calibrations. This conclusion is supported by the results of Doelling *et al.* [2004] who observed 8 and 3% differences between MODIS-Terra and SEVIRI reflectances for the 0.6  $\mu\text{m}$  and 1.6  $\mu\text{m}$  channels, respectively.

The comparison of SEVIRI and AVHRR retrieved cloud properties, using operational calibrations, showed an acceptable agreement with respect to variance, whereas the absolute values agreed well for COT and poorly for CLWP. Over the period 15 April until 14 May 2004 SEVIRI retrieved ~15% lower median COT values and ~75% lower median CLWP values than AVHRR. In order to exclude differences between both instruments due to calibration the SEVIRI and AVHRR reflectances were recalibrated. The results of the reflectance comparison over Central Africa were used to normalize the AVHRR reflectances to SEVIRI, whereas the results of Doelling *et al.* [2004] were used to adjust these reflectances to absolutely calibrated MODIS-Terra reflectances. The recalibration did significantly improve the relationship between SEVIRI and AVHRR retrieved cloud properties, with differences dropping to values smaller than 5%. The adjustment of the normalized reflectances to MODIS-Terra reflectances had a significant effect on the magnitude of the cloud property retrievals. The median COT and CLWP values retrieved from AVHRR decreased with about 2 and 60%, respectively, whereas the corresponding values from SEVIRI increased with ~10 and ~55%, respectively. These results clearly demonstrate that recalibration is needed to build a consistent dataset of cloud properties from SEVIRI and AVHRR for climate research purposes.

The differences in spatial resolution and viewing geometry have a much smaller effect on the comparability of SEVIRI and AVHRR retrievals. Despite the large difference in spatial

resolutions of SEVIRI and AVHRR, the frequency distributions of cloud properties from both instruments were similar in terms of minimum, mean, maximum and peak values. Only at the low tail of the distributions differences related to broken clouds fields were observed, which can be resolved at the AVHRR resolution but appear as overcast thin clouds at the SEVIRI resolution. Moreover, small differences were observed due to differences in viewing geometry. This is consistent with the findings of *Loeb and Coakley* [1998], who expect no systematic bias in cloud property retrievals for the viewing conditions considered in this study i.e.: solar zenith angles were smaller than  $60^\circ$  and relative azimuth angles of about  $140^\circ$ .

However, it is suggested that over North Western Europe the SEVIRI retrievals are more sensitive to errors due to its unfavorable viewing conditions; firstly, because SEVIRI has a large viewing zenith angle over this region, and secondly, because the scattering angle is close to  $180^\circ$ , i.e. backscatter direction, for about 10% of the observations. The analysis of the relationship between satellite viewing zenith angle and DAK simulated reflectances indicated that the uncertainty in cloud property retrieval increases with satellite viewing zenith angle. The satellite viewing zenith angle for which the uncertainties of the retrievals start to increase is solar zenith angle dependent. Since over North Western Europe the viewing zenith angles of SEVIRI are large it is expected that especially for early morning, late afternoon and winter observations the cloud property retrievals from SEVIRI will have a much larger uncertainty than those from AVHRR.

This paper has demonstrated that the CPP algorithm provides robust and consistent estimates of Cloud Liquid Water Path and Cloud Optical Thickness from SEVIRI and AVHRR reflectances. Given the differences between SEVIRI and AVHRR in spectral characteristics, spatial resolution and viewing geometry, the retrieved cloud properties of both instruments compare well over North Western Europe. The large differences that were found between the

calibrations of NOAA-17/AVHRR and METEOSAT-8/SEVIRI highlight the need for a coordinated inter-calibration effort guided by the satellite operators. It has been clearly shown that recalibration is the most important requirement for constructing a uniform dataset of cloud properties for climate research.

**Acknowledgements.** This work was part of the EUMETSAT funded CM-SAF project. The authors like to thank Anke Tetzlaff of SMHI and Max Reuter of the University of Berlin for providing the AVHRR and SEVIRI data for Central Africa, respectively. Moreover, we would like to thank William Rossow who made it possible to do part of the work presented in this paper at the NASA Goddard Institute for Space Studies in New York, USA.

## References

- Anderson, G. P., S. A. Clough, F. X. Kneizys, J. H. Cheywynd, and E. P. Shettle, (1986), AFGL Atmospheric Constituent Profiles (0-120km), *AFGL-TR-86-0110*, ADA175173.
- Cahalan, R. F., W. Ridgway, W. J. Wiscombe, T. L. Bell, and J. B. Snider (1994), The albedo of fractal stratocumulus clouds, *J. Atmos. Sci.*, *51*, 2434-2455.
- Cess, R. D., G. L. Potter, J. P. Blanchet, G. J. Boer, S. J. Ghan, J. T. Kiehl, H. Le Treut, Z.-X. Li, X.-Z. Liang, J. F. B. Mitchell, J.-J. Morcrette, D. A. Randall, M. R. Riches, E. Roeckner, U. Schlese, A. Slingo, K. E. Taylor, W. M. Washington, R. T. Wetherald, and I. Yagai (1989), Interpretation of cloud-climate feedback as produced by 14 atmospheric general circulation models, *Science*, *245*, 513-516.
- Davis, A., A. Marshak, R. Cahalan, and W. Wiscombe (1997), The LANDSAT scale-break in stratocumulus as a three-dimensional radiative transfer effect, implications for cloud remote sensing, *J. Atmos. Sci.*, *54*, 241-260.

- De Haan, J. F., P. Bosma, and J. W. Hovenier (1987), The adding method for multiple scattering calculations of polarized light, *Astron. Astrophys.*, *183*, 371-391.
- Doelling, D. R., L. Nguyen, and P Minnis (2004), Calibration comparisons between SEVIRI, MODIS and GOES data, paper presented at EUMETSAT Meteorological Satellite Data User's Conference, Prague, Czech Republic, 2004.
- Feijt, A.J., D. Jolivet, R. Koelemeijer and H. Deneke (2004), Recent improvements to LWP retrievals from AVHRR, *Atmos. Res.*, *72*, 3-15.
- Govaerts Y. and M. Clerici (2004a), Evaluation of Radiative Transfer Simulations Over Bright Desert Calibration Sites, *IEEE Trans. on Geoscience and Remote Sensing*, *42*, 176-187.
- Govaerts Y. and M. Clerici (2004b), MSG-1/SEVIRI Solar Channels Calibration Commissioning Activity Report, EUM/MSG/TEN/04/0024.
- Guenther B., G. Godden, X. Xiong , E. Knight, S. Qiu S., H. Montgomery, M. Hopkins, M. Khayat , and Z. Hao (1998), Prelaunch algorithm and data format for the level 1 calibration products for the EOS-AM1 moderate resolution image spectroradiometer (MODIS), *IEEE Trans. Geosci. Remote Sensing*, *36*, 1142-1151.
- Han Q, W.B. Rossow, A.A. Lasis (1994), Near-Global Survey of Effective Droplet Radii in Liquid Water Clouds Using ISCCP Data, *J. of Clim.*, *7*, 465-497.
- Hansen, J. E. and J. W. Hovenier (1974), Interpretation of the polarization of Venus, *J. Atmos. Sci.*, *31*, 1137-1160.
- Heidinger, A., C. Cao, and J. Sullivan (2002), Using MODIS to calibrate AVHRR reflectance channels, *J. Geophys. Res.*, *107*, 4702-4711.
- Hess, M., R.B.A. Koelemeijer (1998), P. Stammes, Scattering matrices of imperfect hexagonal ice crystals, *J. Quant. Spectros. Radiative Transfer*, *60*, 301-308.

Intergovernmental Panel on Climate Change (IPCC) Third Assessment Report (TAR) (2001),

*Climate Change 2001: The Scientific Basis*, edited by J. T. Houghton, Y. Ding, D. J. Griggs, M. Noguer, P. J. van der Linden, X. Dai, K. Maskell, and C. A. Johnson, Cambridge Univ. Press, New York.

Jolivet, D. and A. Feijt (2005), Quantification of the accuracy of LWP fields derived from NOAA-16 advanced very high resolution radiometer over three ground stations using microwave radiometers, *J. Geophys. Res.*, *110*, D11204, doi:10.1029/2004JD005205.

Knap, W. H., L. C.-Labonnote, G. Brogniez and P. Stammes. (2005), Modeling total and polarized reflectances of ice clouds: evaluation by means of POLDER and ATSR-2 measurements. *Applied Optics*, *44*, 4060-4073.

King, M.D., S.C. Tsay, S.E. Platnick, M. Wang, and K.N. Liou (1997), MODIS Algorithm Theoretical Basis Document: Cloud Retrieval Algorithms for MODIS: Optical Thickness, Effective Particle Radius, and Thermodynamic Phase, *ATBD-MOD-05*, December 1997.

King, M. D., S. Platnick, P. Yang, G. T. Arnold, M. A. Gray, and J. C. Riédi, S. A. Ackerman, and K. N. Liou (2004), Remote sensing of liquid water and ice cloud optical thickness, and effective radius in the arctic: Application of airborne multispectral MAS data, *J. Atmos. Oceanic Technol.*, *21*, 857-875.

Loeb, N. G. and J. A. Coakley (1998), Inference of Marine Stratus Cloud Optical Depth from Satellite Measurements: Does 1D Theory Apply?, *J. Climate*, *11*, 215–233.

Minnis P., K.N. Liou, and Y. Takano (1993), Inference of Cirrus Cloud Properties Using Satellite-observed Visible and Infrared Radiances. Part I: Parameterization of Radiance Fields, *J. of Atmos. Sciences*, *50*, 1279–1304.

- Nakajima T., and M. D. King (1990), Determination of the Optical Thickness and Effective Particle Radius of Clouds from Reflected Solar Radiation Measurements. Part 1: Theory, *J. of Atmos. Sciences*, 47, 1878-1893.
- Nakajima T. Y., and T. Nakajima (1995), Determination of Cloud Microphysical Properties from NOAA AVHRR Measurements for FIRE and ASTEX regions, *J. of Atmos. Sciences*, 52, 4043 -4059.
- Platnick, S. (2001), A Superposition Technique for deriving Mean Photon Scattering Statistics in Plane-Parallel Cloudy Atmospheres, *Journal of Quantitative Spectroscopy and Radiative Transfer*, 68, 57-73.
- Rao, C.R.N., and J. Chen (1995), Inter-satellite calibration linkages for the visible and near-infrared channels of the Advanced Very High Resolution Radiometer on NOAA-7, -9, and -11 spacecraft, *International Journal of Remote Sensing*, 16, 1931-1942.
- Roebeling, R.A., A. Berk, A.J. Feijt, W. Frerichs, D. Jolivet, A. Macke, and P. Stammes (2005), Sensitivity of cloud property retrievals to differences in narrow band radiative transfer simulations, *Sci. Rep WR 2005-02*, Koninklijk Ned. Meteorol. Inst., De Bilt, the Netherlands.
- Rosenfeld, D., E. Cattani, S. Melani, and V. Levizzani. (2004), Considerations on daylight operation of 1.6-versus 3.7- $\mu\text{m}$  channel on NOAA and Metop satellites, *Bull. Amer. Meteor. Soc.*, 85, 873–881.
- Rossow, W.B., and R.A. Schiffer (1991), ISCCP cloud data products, *Bull. Amer. Meteor. Soc.*, 72, 2-20.
- Rossow, W.B., and R.A. Schiffer (1999), Advances in understanding clouds from ISCCP, *Bull. Amer. Meteor. Soc.*, 80, 2261-2287.

- Stammes, P. (2001), Spectral radiance modeling in the UV-Visible range. *IRS 2000: Current problems in Atmospheric Radiation*, edited by W.L. Smith and Y.M. Timofeyev, pp 385-388, A. Deepak Publ., Hampton, Va.
- Stammes P., J.R. Acarreta, W.H. Knap, and L.G. Tilstra (2005), Earth reflectance spectra from 300-1750 nm measured by SCIAMACHY, *IRS 2004: Current Problems in Atmospheric Radiation*, Edited by H. Fischer and B.-J. Sohn, A. Deepak Publishing, Hampton, Va, submitted.
- Stephens G. L., G. W. Paltridge, and C. M. R. Platt (1978), Radiation profiles in extended water clouds. III. Observations, *J. Atmos. Sci.*, 35, 2133-2141.
- Varnai, T., and A. Marshak (2002), Observations of three-dimensional radiative effects that influence MODIS cloud optical thickness retrievals, *J. Atmos. Sci.*, 59, 1607-1618.
- Watts P.D., C.T. Mutlow, A. J. Baran, and A.M. Zavody (1998), Study on Cloud Properties derived from Meteosat Second Generation Observations, Final Report, *EUMETSAT ITT no. 97/181*.
- Wielicki, B. A., and L. Parker, L. (1992), On the Determination of Cloud Cover from Satellite Sensors: The Effect of Sensor Spatial Resolution, *Journal of Geophysical Research*, 97, 12,799 - 12,823.
- Woick, H., Dewitte, S., Feijt, A., Gratzki, A., Hechler, P., Hollmann, R., Karlsson, K.-G., Laine, V., Löwe, P., Nitsche, H., Werscheck, M., and Wollenweber, G. (2002), The Satellite Application Facility on climate monitoring, *Adv. Space Res.*, 30, 2405-2410.
- Wu X, and P. W. Michael (2003), Post-launch calibrations of AHVRR and GOES solar channels, CGMS-XXXI Meeting, Ascona, Switzerland, 2003, EUMETSAT publication, *CGMS-XXXI USA-WP-30*.

**Table 1.** Spatial and spectral characteristics of SEVIRI and AVHRR visible and near-infrared channels.

<i>Channel</i>	<i>SEVIRI</i>		<i>AVHRR</i>	
	<i>res. nadir (km)</i>	<i>spectral band (<math>\mu\text{m}</math>)</i>	<i>res. nadir (km)</i>	<i>spectral band (<math>\mu\text{m}</math>)</i>
<b><i>VIS 0.6</i></b>	3	0.56 - 0.71	1.1	0.58 - 0.68
<b><i>VIS 0.8</i></b>	3	0.74 - 0.88	1.1	0.73 - 1.00
<b><i>NIR 1.6*</i></b>	3	1.50 - 1.78	1.1	1.58 - 1.64
<b><i>NIR 3.8*</i></b>	3	3.48 - 4.36	1.1	3.55 - 3.93

\* The NOAA-17 AVHRR NIR 1.6 channel is active during daytime, while the NIR 3.8 channel is active during nighttime.

**Table 2.** SEVIRI and AVHRR 0.6 and 1.6  $\mu\text{m}$  channel reflectances calculated from TOA SCIAMACHY reflectance spectra for 5 typical surfaces (ocean, vegetation, desert, liquid cloud and cirrus cloud). The differences due to bandwidth and spectral response function of SEVIRI reflectances relative to AVHRR reflectances are given in %.

	<i>Position</i>		<i>0.6 <math>\mu\text{m}</math> channel</i>			<i>1.6 <math>\mu\text{m}</math> channel</i>		
	<i>latitude</i>	<i>longitude</i>	<i>SEVIRI</i>	<i>AVHRR</i>	<i>% Difference</i>	<i>SEVIRI</i>	<i>AVHRR</i>	<i>% Difference</i>
<i>Sea</i>	45.2	-4.4	0.0386	0.0393	-1.8	0.0104	0.0096	7.7
<i>Vegetation</i>	53.9	28.6	0.0629	0.0634	-0.8	0.1471	0.1451	4.2
<i>Desert</i>	31.1	17.7	0.3353	0.3284	2.1	0.5425	0.5391	0.6
<i>Liquid cloud</i>	60.1	-2.7	0.5066	0.5014	1.0	0.4323	0.4222	2.4
<i>Cirrus cloud</i>	14.8	-15.4	0.6094	0.6075	0.3	0.1853	0.1666	11.2

**Table 3.** Properties of the cloudy atmosphere and the surface that are used for the radiative transfer calculations to generate the LUTs.

<i>Parameter</i>	<i>Settings</i>	
Atmospheric vertical profiles of pressure temperature and ozone	Midlatitude summer <sup>a</sup>	
Aerosol model	none	
Cloud height	1000 - 2000 m	
Solar zenith angle ( $\theta_0$ )	0 - 75°	
Viewing zenith angle ( $\theta$ )	0 - 75°	
Relative azimuth angle ( $\phi$ )	0 - 180°	
Cloud Optical Thicknesses	0 - 128	
Surface albedo (ocean)	0.05 (0.6 $\mu\text{m}$ ), 0.05 (1.6 $\mu\text{m}$ )	
Surface albedo (land)	0.10 (0.6 $\mu\text{m}$ ), 0.10 (1.6 $\mu\text{m}$ )	
	<u><i>water clouds</i></u>	<u><i>ice clouds</i></u>
Cloud particle type	Spherical water droplet	Imperfect hexagonal ice crystal <sup>b</sup>
Cloud particle size	1 - 24 $\mu\text{m}$	C1: L=30, D=20 $\mu\text{m}$ <sup>c</sup> C2: L=60, D=44 $\mu\text{m}$ <sup>c</sup>
Size distribution	Modified gamma	-
Effective variance ( $v_e$ )	0.15	-

<sup>a</sup> The midlatitude summer atmosphere model was taken from *Anderson et al.* [1986].

<sup>b</sup> The imperfect hexagonal crystals are obtained from *Hess et al.* [1998] and have a distortion angle of 30°.

<sup>c</sup> L and D are the length and the diameter of the hexagon, respectively.

**Table 4.** The median and 95<sup>th</sup> percentile of COT and CLWP for water clouds from AVHRR and SEVIRI for the period 15 April until 14 May 2004, using the operational calibrations. The correlation coefficients ( $r$ ) and standard deviation of differences of AVHRR and SEVIRI retrieved COT and CLWP for the 35 images of the observation period are given.

	<i>median</i>				<i>95<sup>th</sup> percentile</i>			
	<i>AVHRR</i>	<i>SEVIRI</i>	<i>r</i>	<i>Std_Diff</i>	<i>AVHRR</i>	<i>SEVIRI</i>	<i>r</i>	<i>Std_Diff</i>
<b><i>COT</i></b>	8.7	7.5	0.96	1.5	38.7	33.5	0.84	5.9
<b><i>CLWP</i></b>	91.5	24.3	0.92	33.6	482.3	287.4	0.83	71.6

**Table 5.** The median and 95<sup>th</sup> percentile of COT and CLWP for water clouds from AVHRR and SEVIRI for the period 15 April until 14 May 2004, using recalibrated reflectances. The correlation coefficients ( $r$ ) and standard deviation of differences of AVHRR and SEVIRI retrieved COT and CLWP for the 35 images of the observation period are given.

	<i>median</i>				<i>95<sup>th</sup> percentile</i>			
	<i>AVHRR</i>	<i>SEVIRI</i>	<i>r</i>	<i>Std_Diff</i>	<i>AVHRR</i>	<i>SEVIRI</i>	<i>r</i>	<i>Std_Diff</i>
<b><i>COT</i></b>	8.5	8.3	0.98	1.4	53.0	55.5	0.91	8.9
<b><i>CLWP</i></b>	35.7	37.5	0.97	11.7	436.9	451.0	0.90	89.3

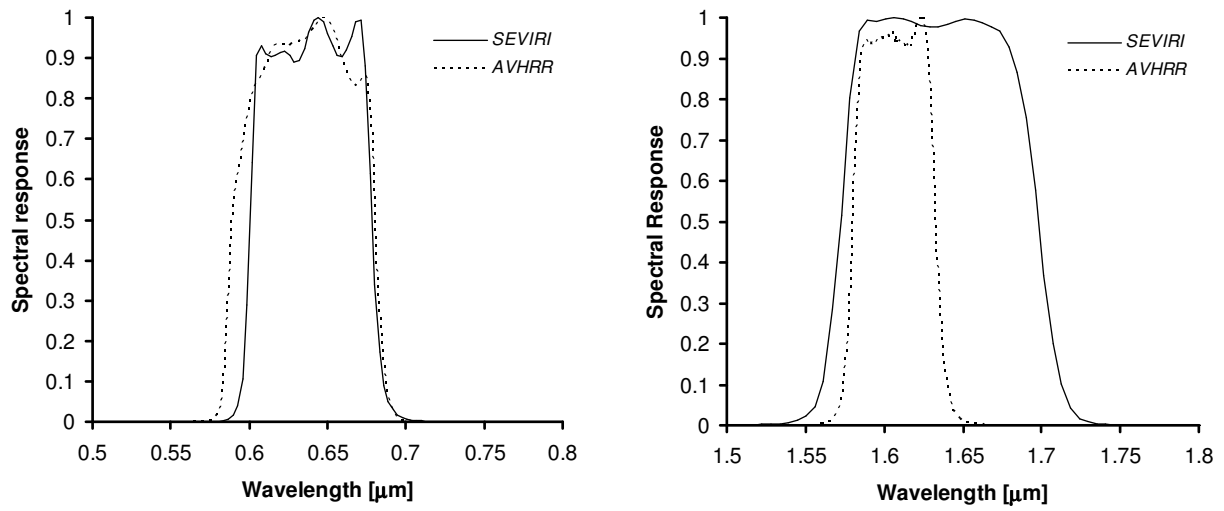


**Figure 1.** Spectral response functions for the SEVIRI and AVHRR 0.6 μm (left) and 1.6 μm (right) channels.

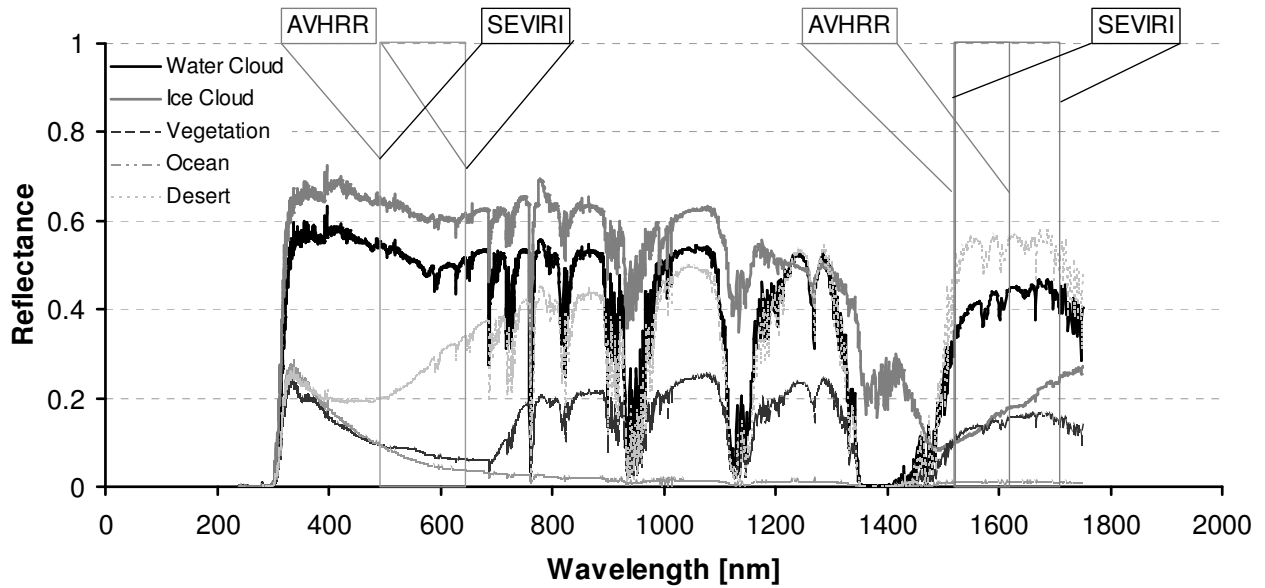


**Figure 2.** SCIAMACHY measured TOA reflectance spectra for 5 typical scenes (ocean, vegetation, desert, liquid cloud and cirrus cloud). The gray blocks indicate the positions of the 0.6 and 1.6  $\mu\text{m}$  channels of SEVIRI and AVHRR.

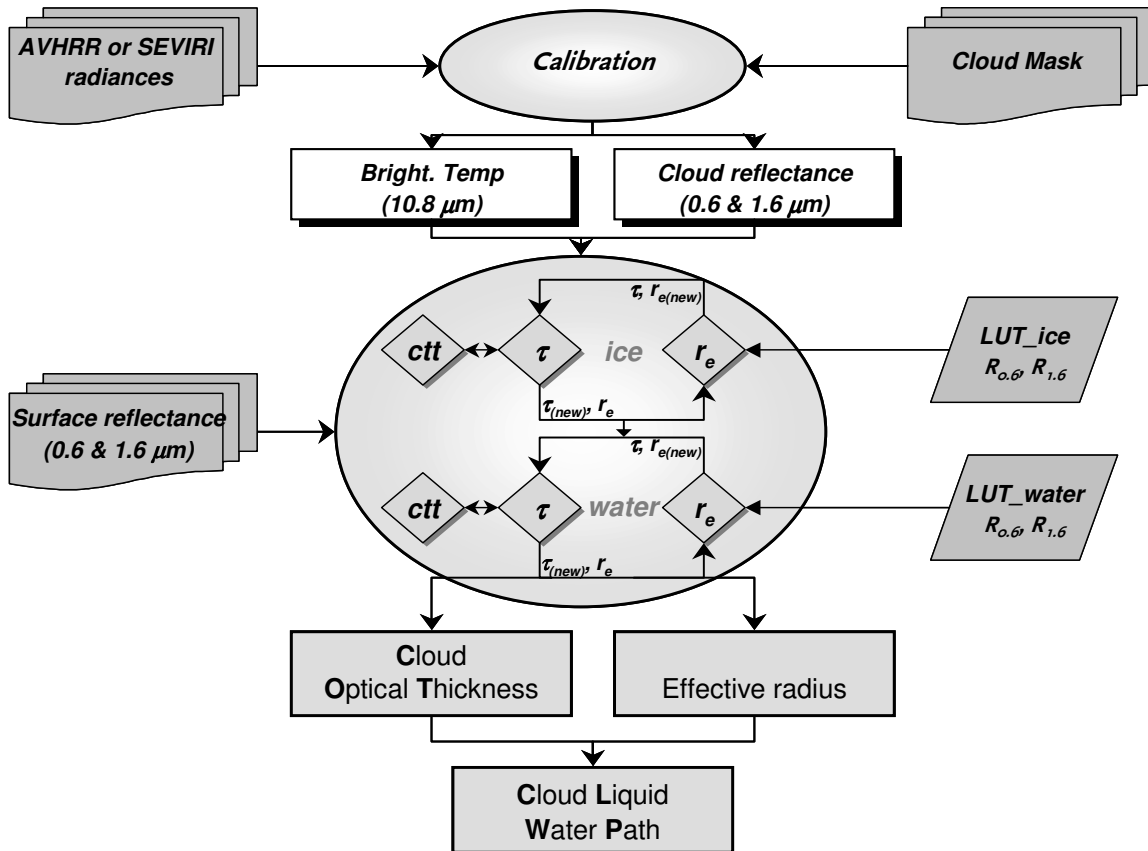


**Figure 3.** Flowchart of CPP algorithm for determining COT ( $\tau$ ), particle size ( $r_e$ ) and CLWP using LUTs of DAK simulated 0.6 and 1.6  $\mu\text{m}$  reflectances and cloud top temperatures (CTT) derived from 10.8  $\mu\text{m}$  brightness temperatures and COT.

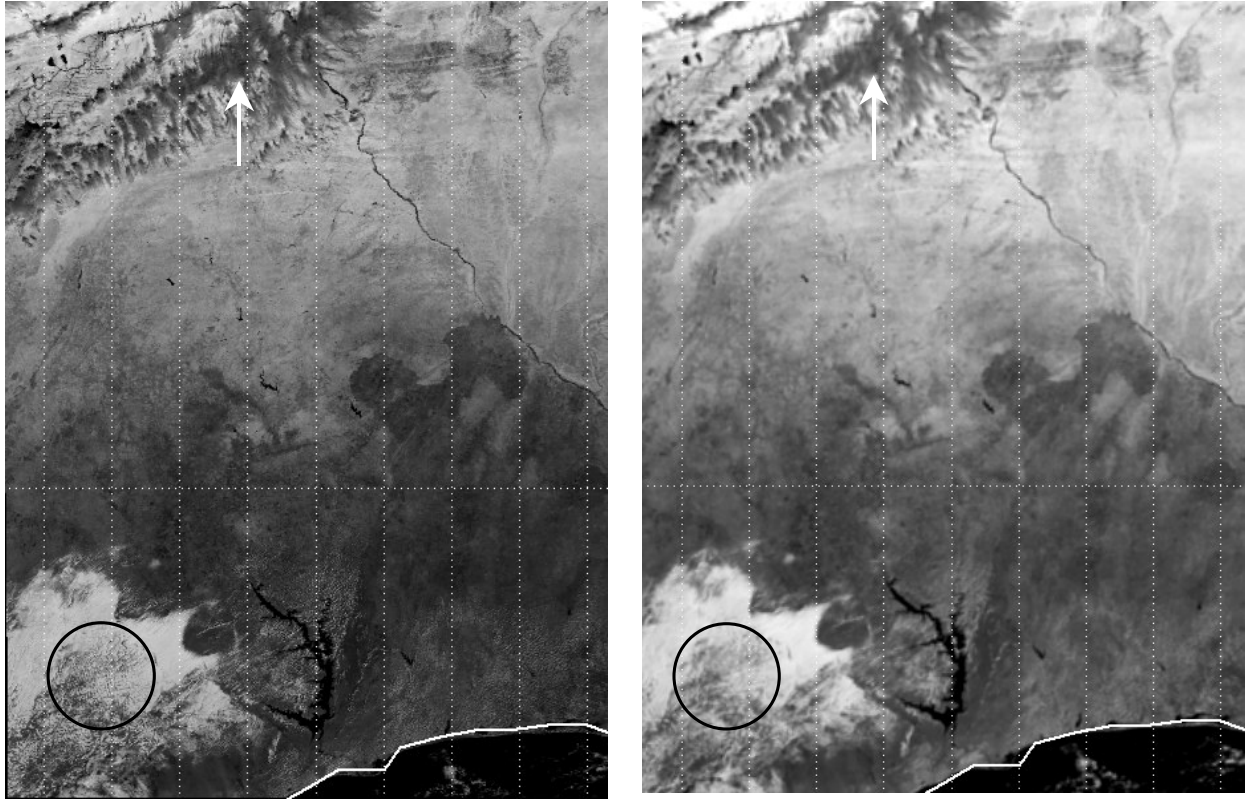


**Figure 4.** AVHRR (left) and SEVIRI (right) 1.6  $\mu\text{m}$  reflectances over Central Africa (5°W to 5°E and 5°N to 18°N) for 25 December 2004 at 10.30 UTC.

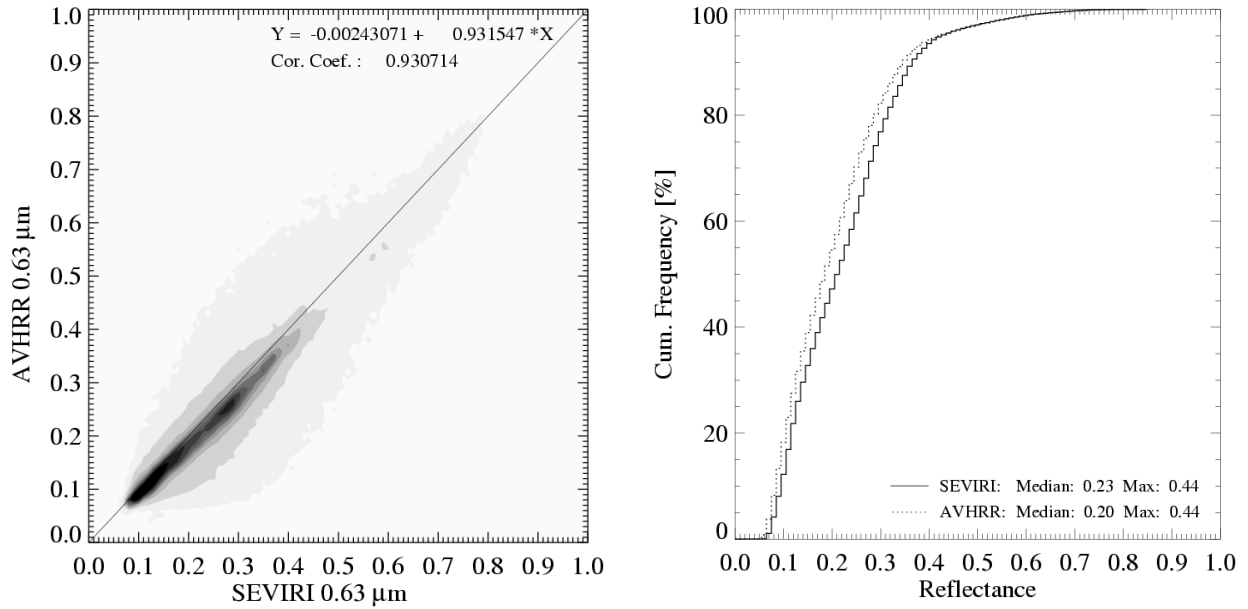


**Figure 5.** Contour plot (left) and cumulative frequency distribution (right) of SEVIRI and AVHRR reflectances for the 0.6 μm channel for 17 images over Central Africa during the period September – December 2004. In the left panel the linear regression equation and correlation coefficient of the contour plot are given and the solid line is the 1:1 line. In the right panel the median and 95<sup>th</sup> percentile (maximum) of the cumulative frequency distribution are given.

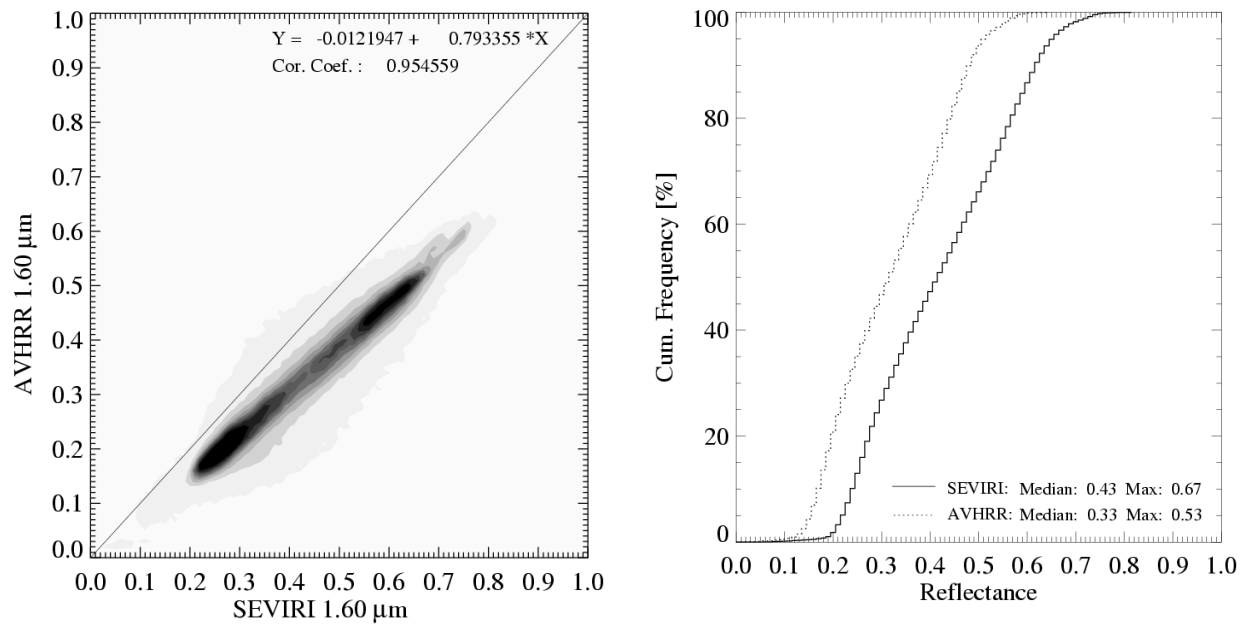


**Figure 6.** Same as Figure 5 but for the 1.6 μm channel.

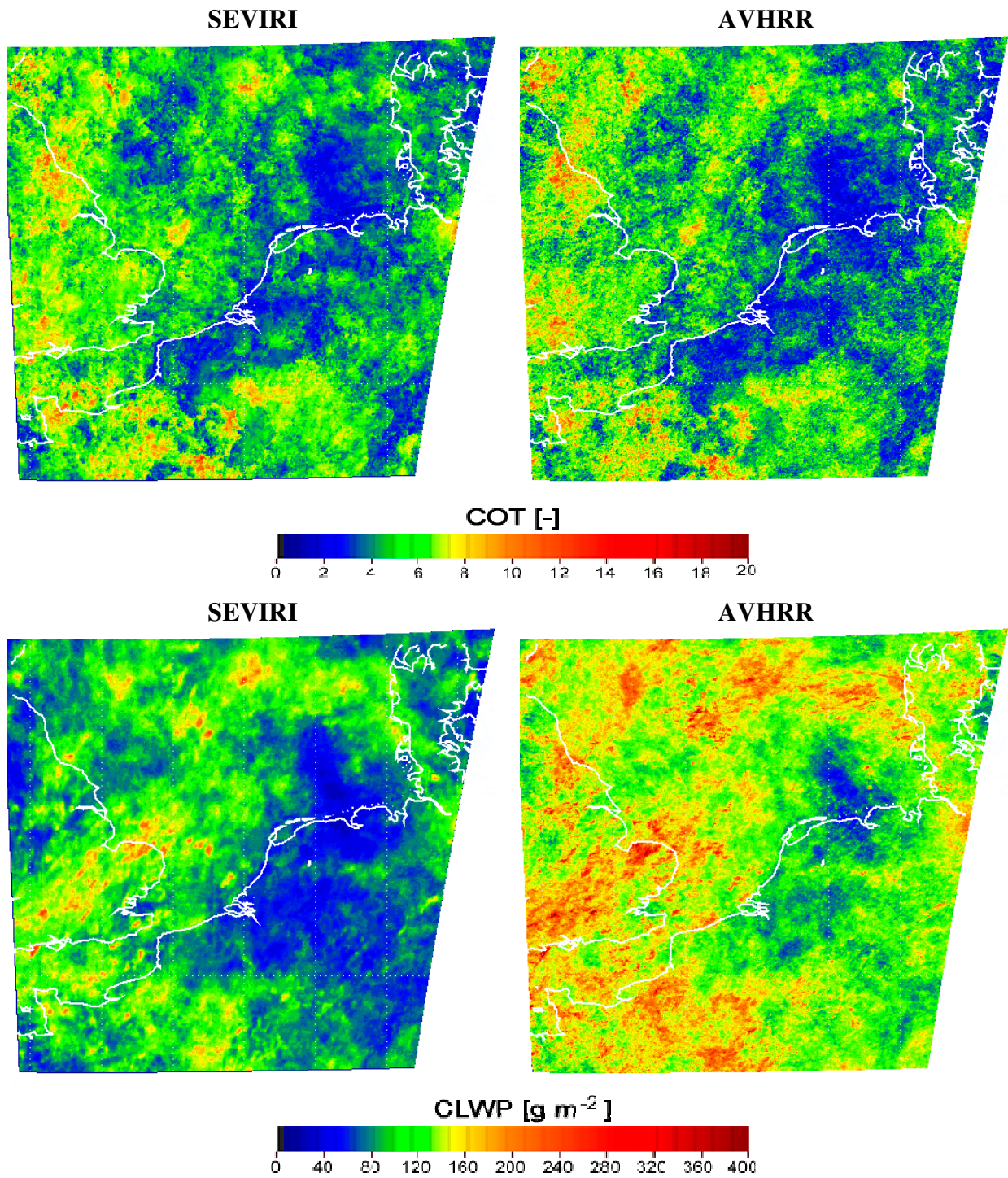


**Figure 7.** Composites of SEVIRI and AVHRR retrieved logarithmic averaged COT (upper) and averaged CLWP (lower) over North Western Europe ( 2.5°W to 11.0°E and 47.5°N to 57.0°N) for water and ice clouds for 35 images during the period 15 April until 14 May 2004.

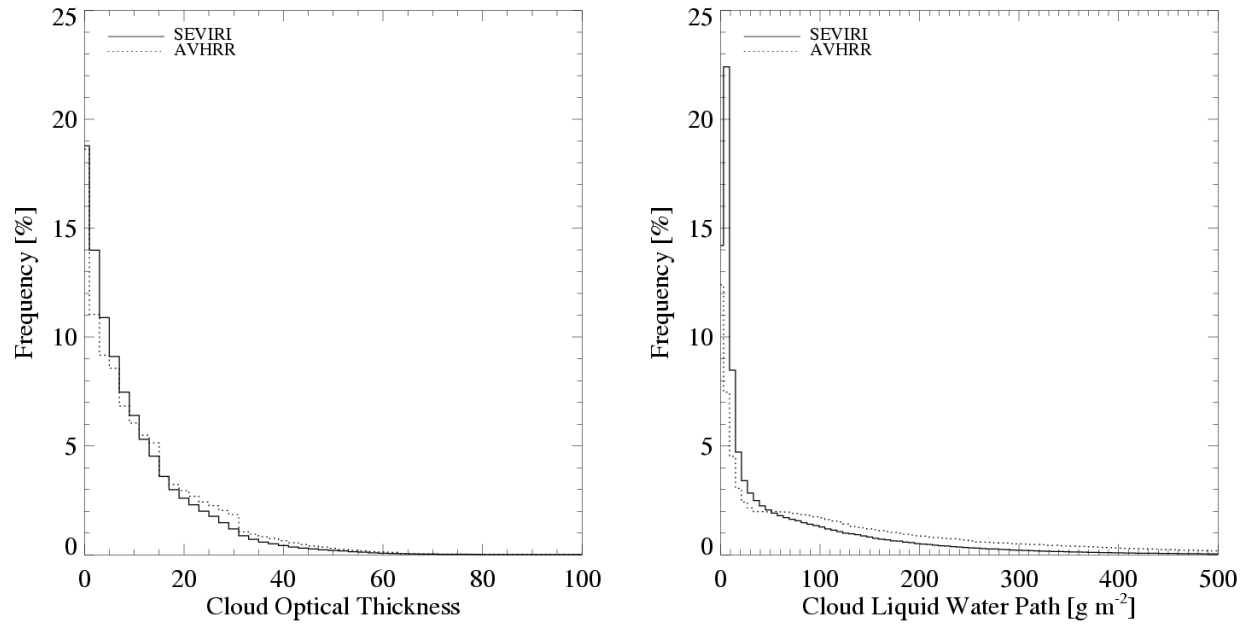


**Figure 8.** Frequency distributions of COT (left) and CLWP (right) retrievals from SEVIRI and AVHRR for water clouds for 35 images during the period 15 April until 14 May 2004, using operational calibrations.

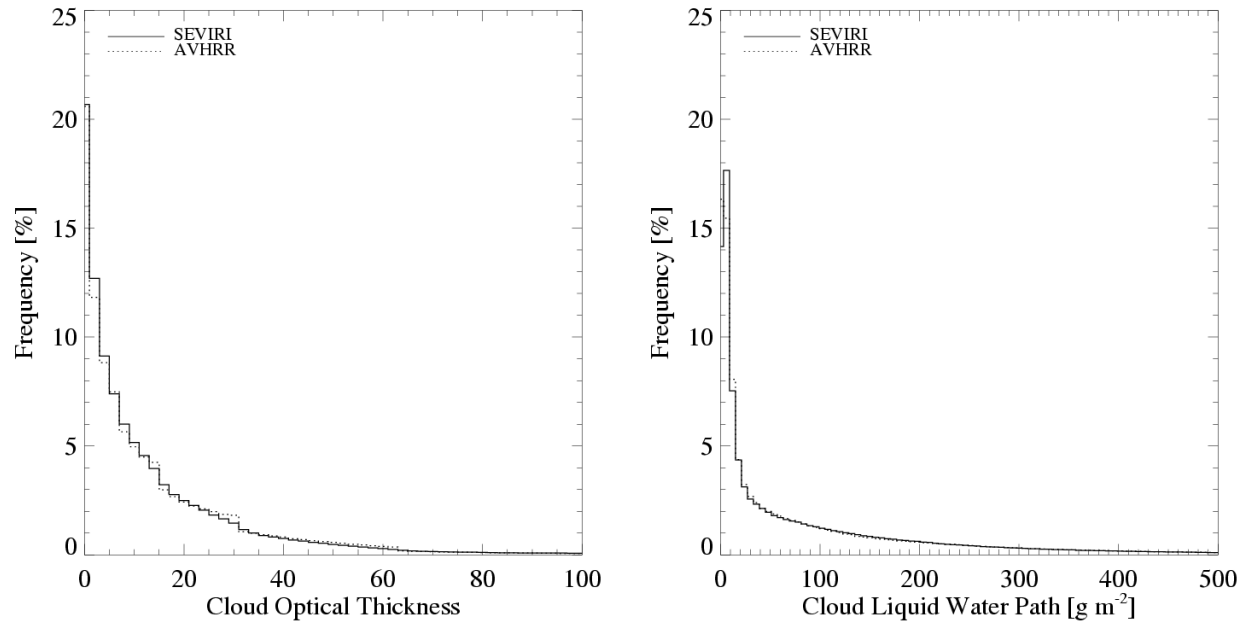


**Figure 9.** Same as Figure 8 but then using recalibrated reflectances for the COT and CLWP retrievals.

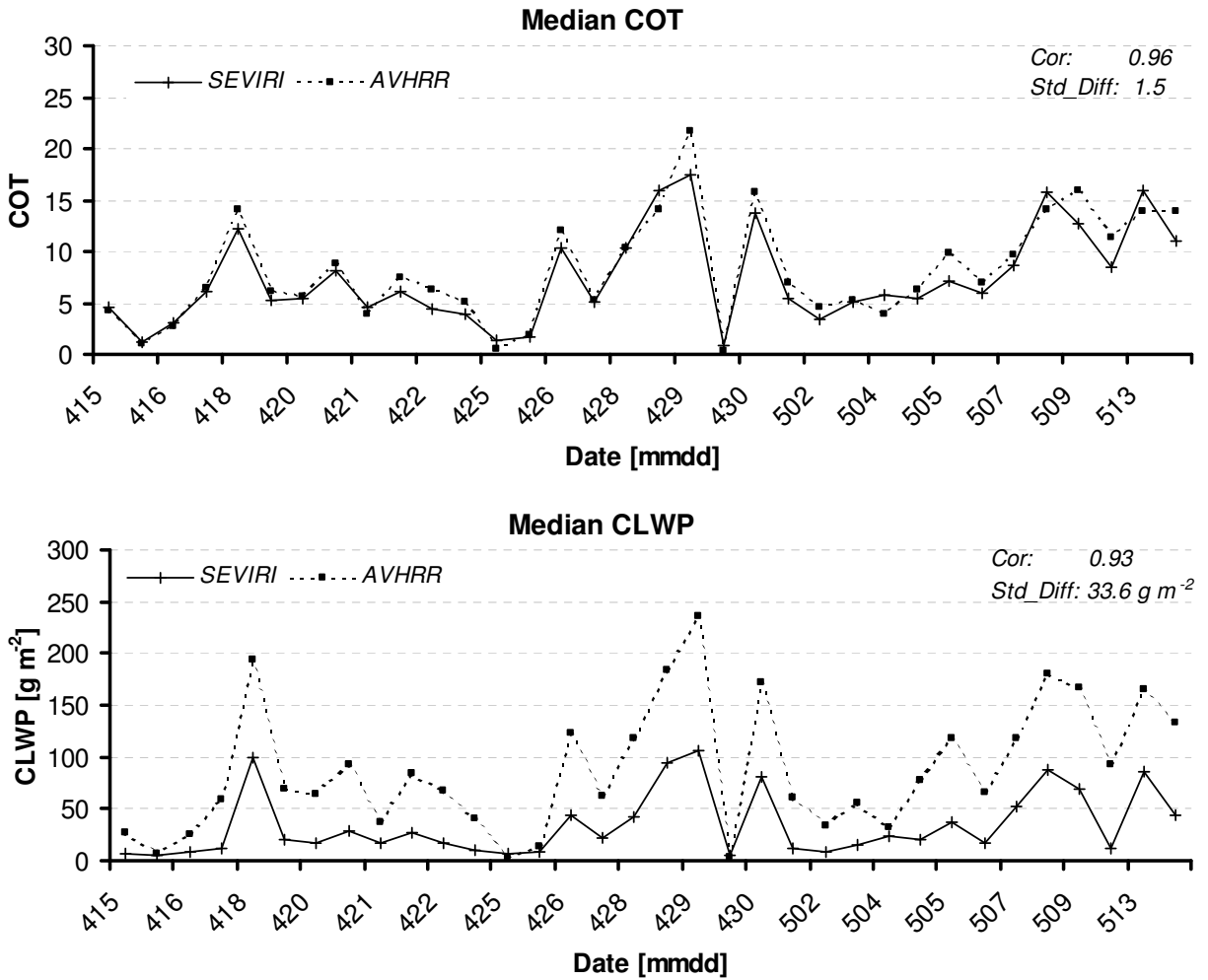


**Figure 10.** Median of frequency distributions of COT and CLWP derived from SEVIRI and AVHRR during the period 15 April 2004 until 14 May 2004, using operational calibrations. In the graphs the correlation coefficients and the standard deviation of the differences are given.

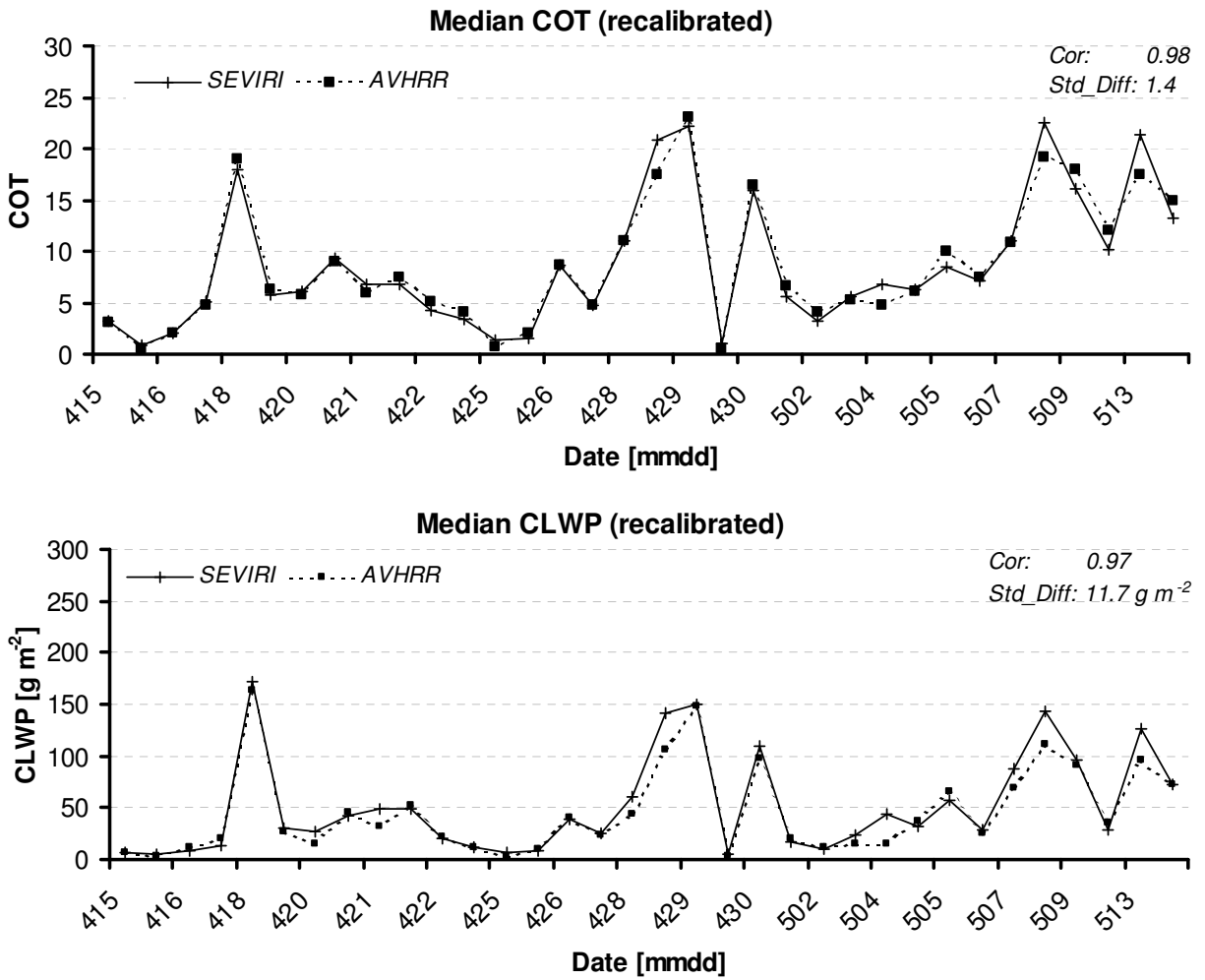


**Figure 11.** Same as Figure 10 but using recalibrated reflectances for the COT and CLWP retrievals.

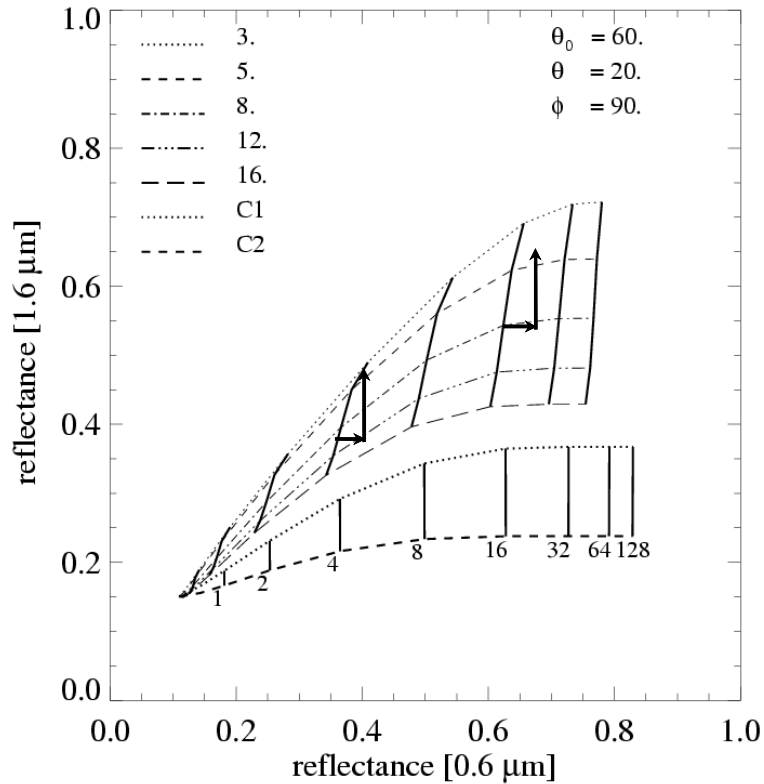


**Figure 12.** Computed DAK reflectances at  $1.6 \mu\text{m}$  versus  $0.6 \mu\text{m}$  for clouds with optical thickness values between 0 and 128 (solid vertical lines) and with effective radii between 3 and  $24 \mu\text{m}$  for water clouds and C1 and C2 imperfect hexagonal columns for ice clouds (dashed-dotted more or less horizontal lines). The results are presented for viewing geometry:  $\theta_0 = 60^\circ$ ,  $\theta = 20^\circ$ ,  $\phi = 90^\circ$  (scattering angle  $\sim 120^\circ$ ). The arrows indicate the impact of 11 and 25% difference in  $0.6 \mu\text{m}$  and  $1.6 \mu\text{m}$  reflectances, respectively.

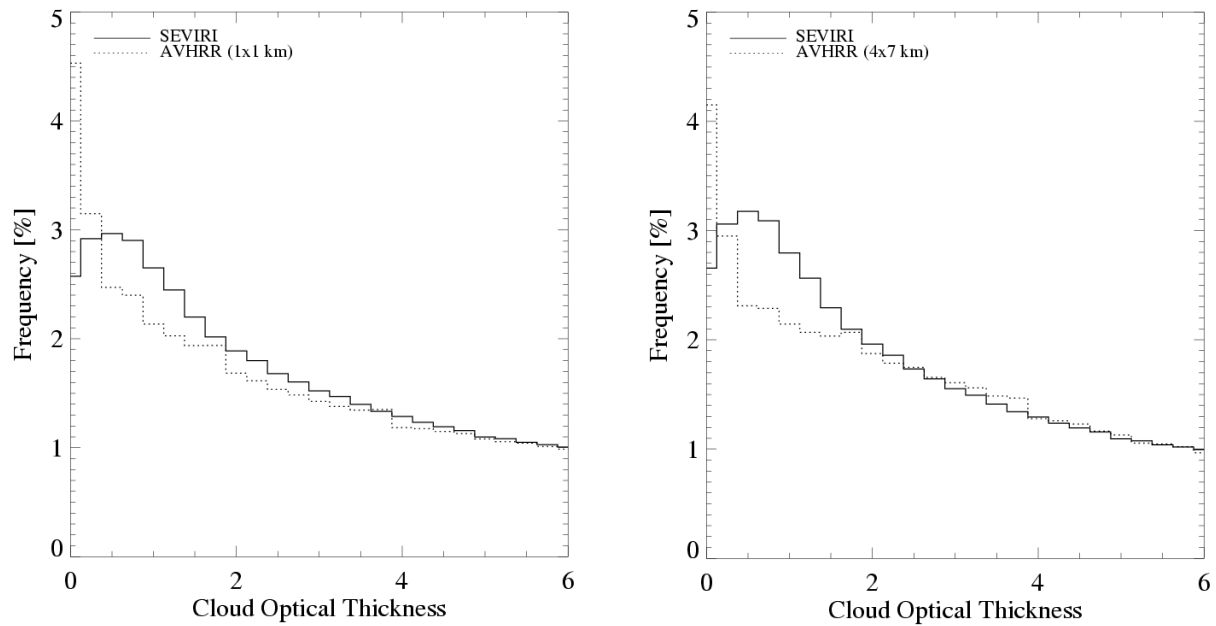


**Figure 13.** Low tail of the frequency distributions of SEVIRI and AVHRR retrieved COT values for water clouds for the period 15 April until 14 May 2004. The COT values from AVHRR were retrieved with full spatial resolution ( $1 \times 1 \text{ km}^2$ ) (left) and resampled spatial resolution ( $4 \times 7 \text{ km}^2$ ) (right), the SEVIRI products were retrieved with recalibrated SEVIRI reflectances.

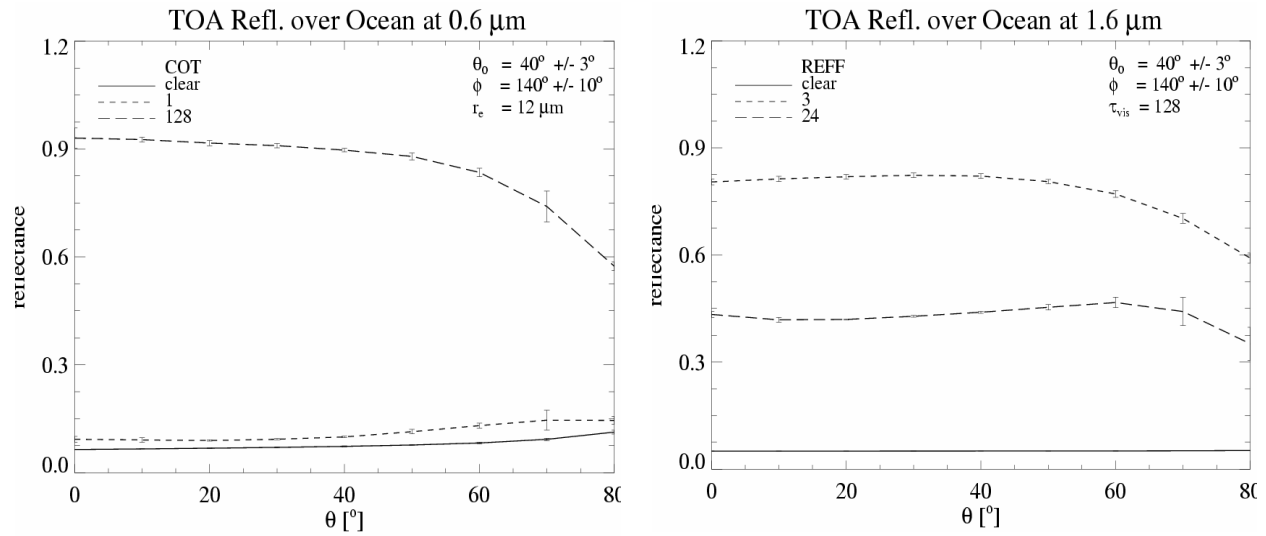


**Figure 14.** The dependence of mean simulated reflectances on satellite viewing angle ( $\theta$ ) over a dark surface, averaged over solar zenith angles ( $\theta_0$ )  $37^\circ$ – $43^\circ$  and relative azimuth angles ( $\phi$ )  $130^\circ$ – $150^\circ$ . In the left panel the  $0.6 \mu\text{m}$  reflectances for clear sky and water clouds with  $\text{COT} = 1$  and 128 and droplet effective radius ( $r_e$ ) =  $12 \mu\text{m}$ , and in the right panel the  $1.6 \mu\text{m}$  reflectances for clear sky and water clouds with  $r_e = 3$  and  $24 \mu\text{m}$  and  $\text{COT} = 128$ . The error bars represent the standard deviation of the mean reflectances.